Nuclear Science and Techniques (2026) 37:67
https://doi.org/10.1007/s41365-026-01886-6

Removal of U(VI) from aqueous solution by layered cobalt–magnesium double hydroxide composite

Meng-Yue Ma[1,2,3] · Yi-Shuo Zhang[1,2,3] · Kun Li[1,2,3] · Guan-Chao Li[4] · Hao-Nan Li[1,2,3] · Xiao-Liang Liu[1,2,3] · Yan-Jun Du[1,2,3] · Muhammad Saeed[5] · Xiao-Yan Li[1,2,3] · Yu-Hui Liu[1,2,3] · Yi-Bao Liu[1,2,3]

Received: 21 July 2024 / Revised: 17 October 2024 / Accepted: 28 October 2024 / Published online: 31 January 2026

Abstract

A novel layered cobalt–magnesium double hydroxide composite (L-CMs) was successfully prepared using a simple one-step co-precipitation method. Static adsorption experiments were conducted to examine the removal efficacy of U(VI) from aqueous solutions by the L-CMs and analyze the removal mechanism. L-CMs efficiently removed U(VI) from the aqueous solution under an adsorption time of 60 min, dosage of 0.4 g/L, and pH of 5.5 at room temperature, and the removal efficiency of U(VI) reached 94.59% with an initial U(VI) concentration of 10 mg/L. The adsorption process was fitted to the pseudo-second-order kinetic and Langmuir models, indicating that monolayer chemical adsorption occurred primarily. The maximum adsorption capacity fitted using the Langmuir model was 105.49 mg/g. Thermodynamic analysis revealed that U(VI) adsorption by L-CMs was endothermic. Structural characterization results showed that the primary mechanism involved the complexation of U(VI) by –OH, CO_3^{2-} and ion exchange by Mg^{2+} and the presence of layered $Co(OH)_2$ in the L-CMs, which potentially facilitated ion exchange. The preparation of the composite materials was simple, and the synergistic effect between the materials enhanced the ion exchange of Mg^{2+} in the materials and enriched the content of functional groups, making it a potential candidate for the treatment of uranium-containing wastewater.

Keywords Adsorption · Uranium · Property · Mechanism · Environmental governance

1 Introduction

Uranium is considered as the "granary" of the nuclear industry, and the demand for uranium is increasing annually [1–3] with the rapid development of the nuclear industry. To satisfy this growing demand, uranium extraction must be intensified. However, the large amounts of radioactive

This work was financially supported by the National Natural Science Foundation of China (Nos. 22266003, 22006013, and 12005037), Academic and Technical Leaders of Major Disciplines in Jiangxi Province (20225BCJ23020), and Graduate Science and Technology Innovation Project of Jiangxi Province (YC2023-S563).

✉ Xiao-Yan Li
372040739@qq.com

✉ Yu-Hui Liu
liuyuhuishui@163.com

✉ Yi-Bao Liu
2968226791@qq.com

[1] Jiangxi Province Key Laboratory of Nuclear Physics and Technology, East China University of Technology, Nanchang 330013, China

[2] Jiangxi Engineering Technology Research Center of Nuclear Radiation Detection and Application, East China University of Technology, Nanchang 330013, China

[3] State Key Laboratory of Nuclear Resources and Environment, East China University of Technology, Nanchang 330013, China

[4] Radiation Environment Monitoring Center of Guangdong Geological Bureau of Nuclear Industry, Guangzhou 510800, China

[5] Yangtze Delta Region Institute (Huzhou), University of Electronic Science and Technology of China, Huzhou 313001, China

uranium-containing wastewater generated during uranium mining, smelting, and nuclear fuel element manufacturing [4, 5] pose risks to human health and the environment [6]. To ensure the rational use and recycling of uranium resources, minimize their ecological impact, and promote sustainable development in both the energy and environmental sectors, an efficient method of treating uranium-containing radioactive wastewater is urgently required [7, 8].

Currently, treatment methods for uranium-containing wastewater primarily include chemical precipitation [9], membrane filtration [10], extraction [11, 12], photocatalytic reduction [13], and adsorption [14, 15]. The adsorption method has attracted attention because of its simplicity, high efficiency, and cost-effectiveness [16–18]. The common adsorbents include activated carbon [19], clay-based materials [20, 21], metal–organic framework [10], and double hydroxides [22]. In recent years, layered double hydroxides (LDHs) have been widely used to treat wastewater containing metal ions, because of their excellent adsorption ability, straightforward operational procedures, and economic advantages [23]. Compared to traditional magnesium–aluminum double hydroxides, new trends exist in the synthesis and application of hydroxides with different compositions [24–27]. $Co(OH)_2$ has a special layered structure similar to that of hydrotalcite (LDHs), and the treatment of organic pollutants and heavy metal ions such as As^{3+} in water has been reported [28–32]. However, reports on the removal of U(VI) by $Co(OH)_2$ are lacking. $Mg(OH)_2$ has a white, hexagonal, and columnar crystal structure and is abundant in nature. Its environmental friendliness makes it an excellent choice for heavy metal removal [33, 34]. However, $Mg(OH)_2$ exhibits limitations in effectively removing metal pollutants from wastewater, and excessive dosages can potentially lead to reverse dissolution, thereby diminishing the pollutant removal efficiency [35]. Previous studies have focused on modifying LDHs to treat uranium-containing radioactive wastewater, which requires complex preparation methods and limits the research scope of bimetallic hydroxides. Moreover, certain modifiers may cause secondary environmental pollution.

Therefore, to expand the application scope of bimetallic hydroxides, simplify their preparation, solve the problem of self-dissolution caused by the excessive addition of $Mg(OH)_2$, and fully utilize the unique structure of $Co(OH)_2$, combined with previous literature reports [36, 37], the introduction of Co^{2+} could strengthen the layered structure of $Mg(OH)_2$, allow its complete exposure to the surface of the material, enhance the adsorption active sites, and accelerate the ion exchange between Mg^{2+} and U(VI). Consequently, the feasibility of further adding Co species to $Mg(OH)_2$ requires investigation and is significant for improving the removal performance of monomer materials. In addition, the composite material demonstrates a higher presence of adsorption functional groups than the monomeric material, which enhances the efficacy of U(VI) removal.

In this study, a novel layered cobalt–magnesium double hydroxide material (L-CMs) was synthesized by introducing Co^{2+} into $Mg(OH)_2$ layers using a one-step co-precipitation method. To further investigate the removal performance and mechanism of the L-CMs on U(VI), analytical methods such as batch experiments, adsorption model fitting, and contemporary characterization techniques were adopted. The results indicated that unlike conventional LDHs, the L-CMs comprised Co^{2+} and Mg^{2+}, and exhibited excellent removal performance for U(VI). Consequently, the L-CMs was identified as a promising adsorption material for uranium-containing water owing to its distinctive properties.

2 Materials and methods

2.1 Materials

Experimental instrument: Inductively Coupled Plasma Optical Emission Spectrometer Agilent 5100 ICP-OES (Agilent, USA); THZ-C-1 full temperature oscillation box (Taicang Experimental Equipment Factory); CP124C electronic balance (Shanghai Ohaus instrument); 101-3Y constant temperature drying oven (Hangzhou Blue Sky Laboratory Instrument Factory); PHS-3C precision pH meter (Shanghai Zhiguang Instrumentation); 85–2 digital thermostatic magnetic stirrer (Shanghai Instrument Motor); TDL-40B Desktop Centrifuge (Shanghai Anting Scientific Instrument Factory); NC-B ultrapure water equipment (Nike (China)); ESCALAB250 Xi X-ray photoelectron spectroscopy analyzer (SEMALFY); D8-A25 X-ray diffractometer (Bruker, Germany); NNS-450 scanning electron microscope (Czech FEI).

Materials and reagents: $UO_2(NO_3)_2{\cdot}6H_2O$ (97% pure) was procured from Aladdin Biochemical Technology Co., Ltd., China, while hydrochloric acid (purity ≥ 99%), sodium hydroxide (purity ≥ 96.0%), and anhydrous ethanol (purity ≥ 99.7%) were obtained from Xilong Chemical Company, China. Magnesium chloride hexahydrate (≥ 98.0% purity) and cobalt chloride hexahydrate (purity ≥ 99.0%) were procured from Sinopharm, China.

2.2 Preparation of L-CMs

L-CMs was prepared using a simple one-step co-precipitation method. Appropriate amounts of $CoCl_2{\cdot}6H_2O$ and $MgCl_2{\cdot}6H_2O$ were added to deionized water, and the solution pH was adjusted to 12.0. The resulting precipitate was washed, centrifuged, dried in an oven, and ground to obtain the L-CMs adsorbent (Fig. 1).

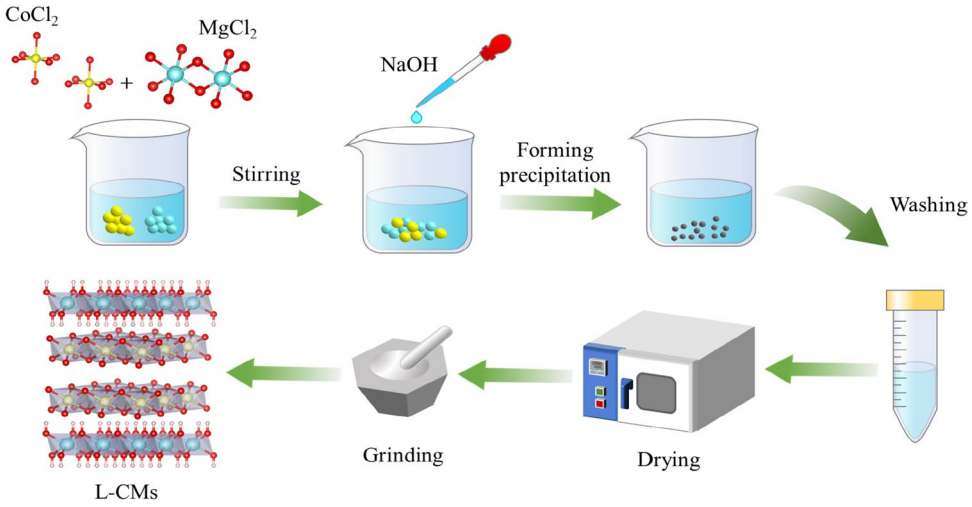

Fig. 1 (Color online) Flowchart for the preparation of L-CMs

2.3 Removal experiments

A specific amount of L-CMs was added to the U(VI) solution, and the initial pH of the solution was adjusted using appropriate concentrations of NaOH and HCl. The reactions were performed at different temperatures for specific durations. After filtration and centrifugation, the uranium content was determined using ICP-OES. The obtained data were used to calculate the removal rate (R) and adsorption capacity (Q_e) using Eqs. (1) and (2):

$$R = \frac{C_0 - C_e}{C_0} \times 100\%, \tag{1}$$

$$Q_e = \frac{(C_0 - C_e)V}{m}, \tag{2}$$

where C_0−U(VI), C_e, V, and m denote the initial concentration (mg/L), concentration of U(VI) in the adsorption equilibrium (mg/L), volume of adsorption material (L), and amount of material (g), respectively.

2.4 Characterization

The prepared L-CMs was characterized by TEM, SEM–EDS, XPS, XRD, and FTIR.

3 Results and discussion

3.1 Characterization analysis of materials

3.1.1 Analysis of the morphology and composition of synthetic materials

The morphology and composition of synthetic materials were analyzed by TEM and SEM–EDS**.** Figure 2 shows that the L-CMs possesses a layered structure similar to that of hydrotalcite-like compounds, and the surface morphology predominantly consists of hexagonal flake-like substances [38]. Notably, the combination of $Mg(OH)_2$ and $Co(OH)_2$ improved aggregation. The layered structure of the L-CMs changed significantly after U(VI) adsorption (Fig. S1 c) owing to the interaction between U(VI) and the L-CMs in the solution. EDS analysis revealed that before adsorption (Fig. S1 b, d), the material contained only Co and Mg. However, the presence of U was detected post-adsorption, thereby confirming successful uranium adsorption by the L-CMs.

3.1.2 Elemental composition and fine analysis of the material

The elemental composition and fine spectrum of the material were analyzed using XPS. The XPS spectra of the L-CMs before and after the adsorption of U(VI) are shown in Fig. 3a-e. The full XPS spectra before and after adsorption are shown in Fig. 3a. Before adsorption, the material primarily consists of Mg, Co, O, and C. After adsorption, a new characteristic peak of U4f appears, which is consistent with the EDS analysis. The fine spectrum of Co2p is shown in Fig. 3b. Before adsorption, the difference between the binding energies of the two main peaks is 15.82 eV, which belongs to the characteristic peak of Co^{2+} indicating that Co exists as Co^{2+}. The Co2p spectrum after adsorption remains almost unchanged, remaining in the form of Co^{2+}, and the peak exhibits no obvious change. Figure 3c shows the fine spectrum of Mg1s. The binding energy before adsorption is 1303.15 eV, indicating that Mg exists as Mg^{2+}. The fine spectrum of Co suggests that the L-CMs consist of divalent metals (Co^{2+} and Mg^{2+}), which differs from previous reports indicating that LDHs are composed of trivalent and divalent metals. After adsorption, the intensity of the Mg^{2+}

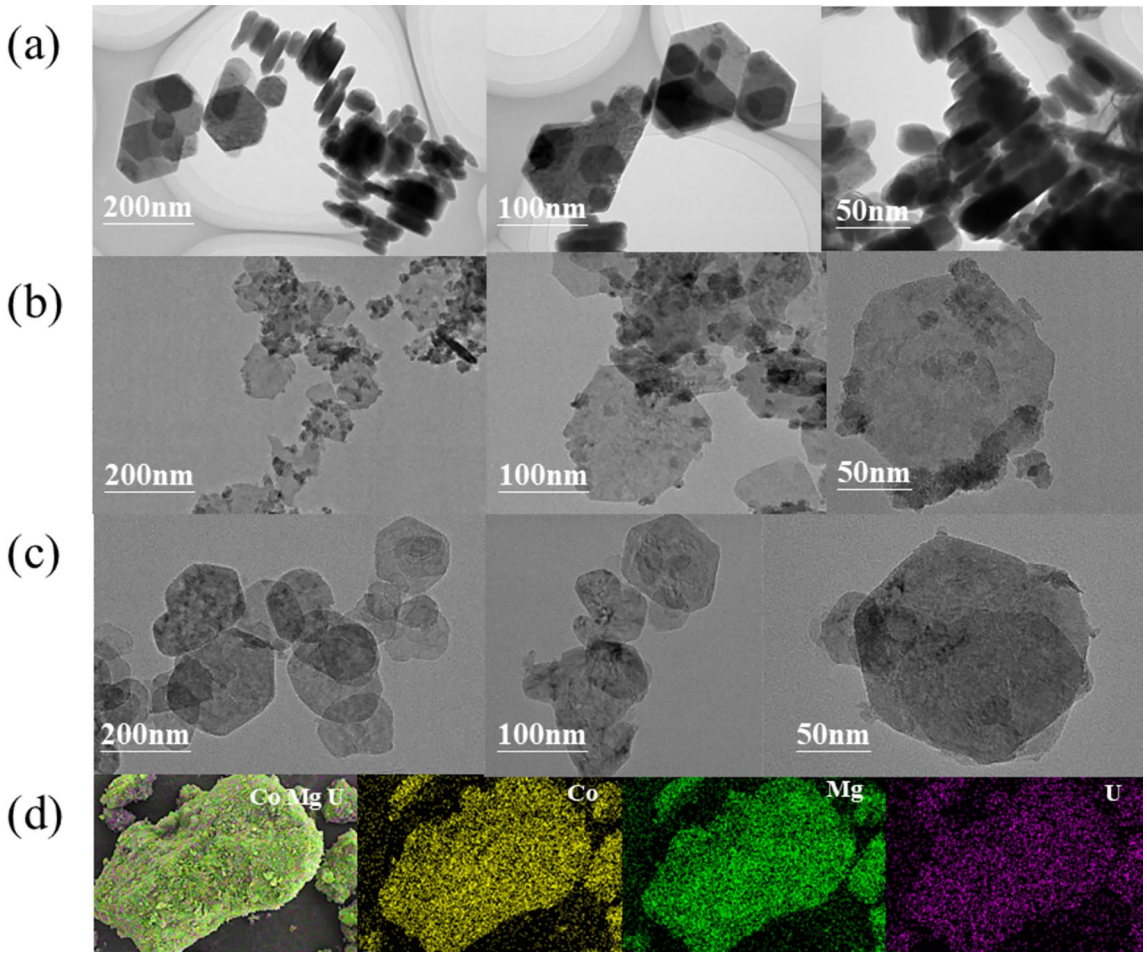

Fig. 2 (Color online) Morphology of **a** $Mg(OH)_2$ from left to right: 500 nm, 200 nm, and 100 nm, **b** $Co(OH)_2$ from left to right: 500 nm, 200 nm, and 100 nm, **c** L-CMs from left to right: 500 nm, 200 nm and 100 nm, **d** EDS of L-CMs-U

peak decreased significantly and the peak position shifted, which was attributed to the decrease in the Mg^{2+} content in the material and the removal of U(VI) by ion exchange. In the fine spectrum of O1s (Fig. 3d), the peak of OH appeared at 531.16 eV, and the peak position of -OH shifted after the reaction, which could be attributed to the complexation between -OH and UO_2^{2+}. In the U4f fine spectrum (Fig. 3e), two main peaks appeared at 381.96 eV and 392.75 eV, indicating the adsorption of U(VI). Therefore, the adsorption mechanism of uranium by the L-CMs may involve the complexation of -OH and exchange of Mg^{2+}.

3.1.3 Phase composition analysis

XRD was performed to analyze the phase composition of the material. As shown in Fig. 3f, the phases of $Co(OH)_2$ (PDF # 74–1057) and $Mg(OH)_2$ (PDF # 44–1482) appeared before adsorption, indicating that the phase of the L-CMs composite primarily comprised $Co(OH)_2$ and $Mg(OH)_2$ of the monomer, and both Co and Mg were divalent. This is consistent with the results of the XPS characterization. After adsorption, the corresponding peak positions of $Co(OH)_2$ and $Mg(OH)_2$ remained unchanged; however, their intensities were significantly reduced, possibly because of the interaction between the L-CMs and U(VI).

3.1.4 Material composition analysis

The material composition of the L-CMs was analyzed using FTIR. The FTIR spectra of the L-CMs before and after U(VI) adsorption are presented in Fig. S3 (g), which shows that the absorption peaks of the sample before adsorption appeared near 3654.03 cm^{-1} and 3456.23 cm^{-1}, respectively, owing to the stretching vibration of the –OH bond in $M(OH)_2$, where M represents Co or Mg. The peak at 479.64 cm^{-1} originated from the stretching vibration of the M–O bond in $M(OH)_2$. The vibration peak of CO_3^{2-} appeared near 1450 cm^{-1}, which could be attributed to the absorption of CO_2 in the air by metal hydroxides. After adsorption, CO_3^{2-} was split into two vibration peaks

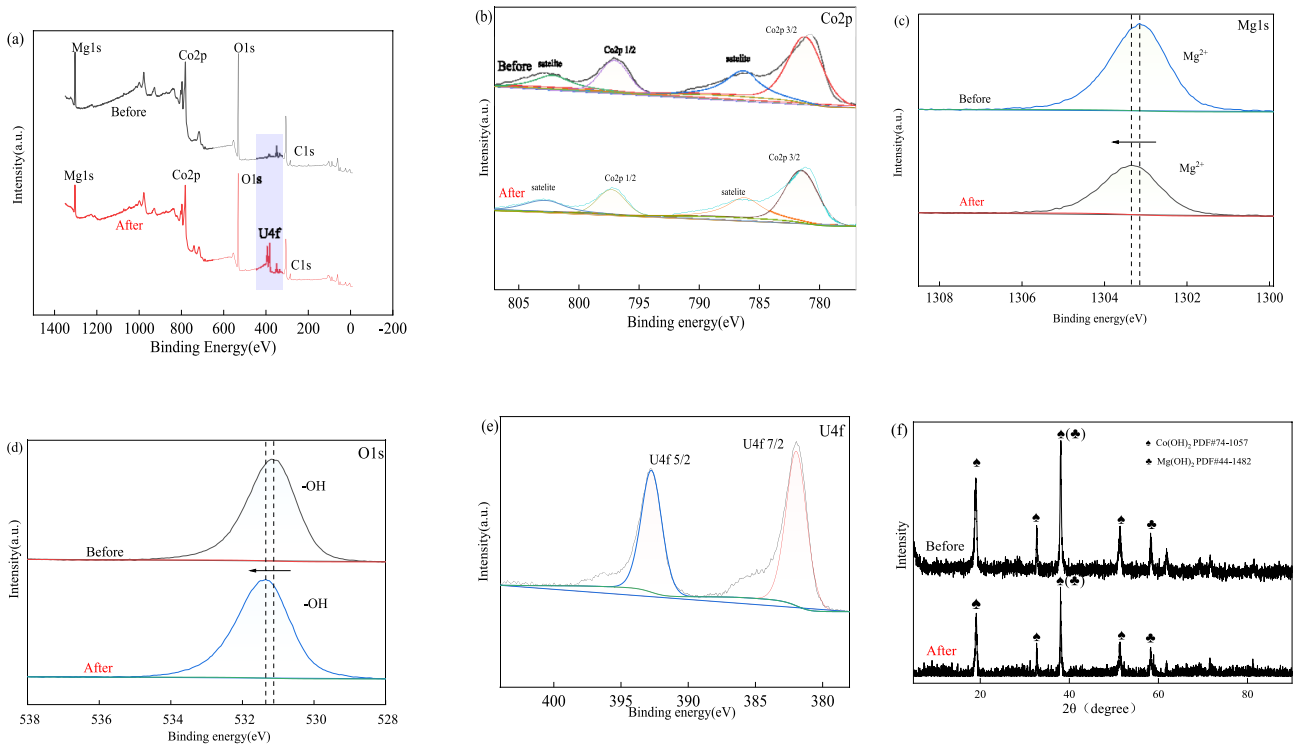

Fig. 3 (Color online) XPS of L-CMS before and after adsorption. **a** Full spectrum, **b** Co2p, **c** Mg1s, **d** O1s, € U4f, **f** XRD before and after adsorption

near 1518 cm^{-1} and 1386 cm^{-1}, indicating that CO_3^{2-} complexed with UO_2^{2+} during the reaction [39]. After adsorption, a characteristic peak belonging to UO_2^{2+} appeared at 906.74 cm^{-1}, which was related to the asymmetric stretching of UO_2^{2+} [40] and indicated that the L-CMs successfully adsorbed U(VI).

3.2 Removal performance of U(VI) by the L-CMs

3.2.1 Effect of preparation condition, solution pH, and dosage of adsorbent

The effect of the cobalt–magnesium ratio on the removal efficiency was examined at a temperature of 25 °C, solution pH of 4.0, and duration of 60 min. The cobalt–magnesium ratio exhibited a discernible influence on the removal of U(VI) (Fig. 4a), and optimal removal efficacy was observed at a Co:Mg ratio of 2:1; hence, this ratio was selected for material synthesis. Notably, the removal efficiency of the composite materials surpassed those of the monomers $Co(OH)_2$ and $Mg(OH)_2$, indicating that the combination of the two enriched the functional groups for U(VI) removal.

The pH of the solution significantly influences the surface charge of the L-CMs [41–43], which is significant for the removal efficiency. Figure 4b shows the effect of the solution pH on the removal of U(VI). The removal rate gradually increases with the solution pH; however, the removal rate decreases when the pH exceeds 5.5. Combined with the surface zeta potential of the L-CMs shown in Fig. 4c, the surface charges of the L-CMs were inferred to be positive at a pH of 2.5. Under these conditions, most of the uranium existed in the form of UO_2^{2+}, the L-CMs did not easily adsorb UO_2^{2+} because of electrostatic repulsion and H^+ competition. As the pH of the solution increased, the positive charge on the surface of the L-CMs gradually decreased, and the competition for H^+ weakened, resulting in increased adsorption capacity. When the solution pH exceeded 5.5, the adsorption capacity of UO_2^{2+} began to decrease, which may be due to the change in the morphological distribution of uranium. Under this condition, uranium mainly exists in the form of $(UO_2)_3(OH)^{7-}$ and $UO_2(OH)^{3-}$, which possess larger ionic radius and lower ion adsorption affinity than UO_2^{2+} [44], and an increase in the solution pH resulted in negative surface charge of the L-CMs. When a large amount of OH^- and UO_2^{2+} are combined, steric hindrance to adsorption occurs [45] resulting in reduced removal efficiency. Therefore, 5.5 was selected as the pH of the solution.

Figure 4d illustrates the effect of adsorbent dosage on U(VI) removal. The removal rate of U(VI) by L-CMs increases gradually with the adsorbent dosage. When the adsorbent dosage reached 0.4 g/L, the removal rate and

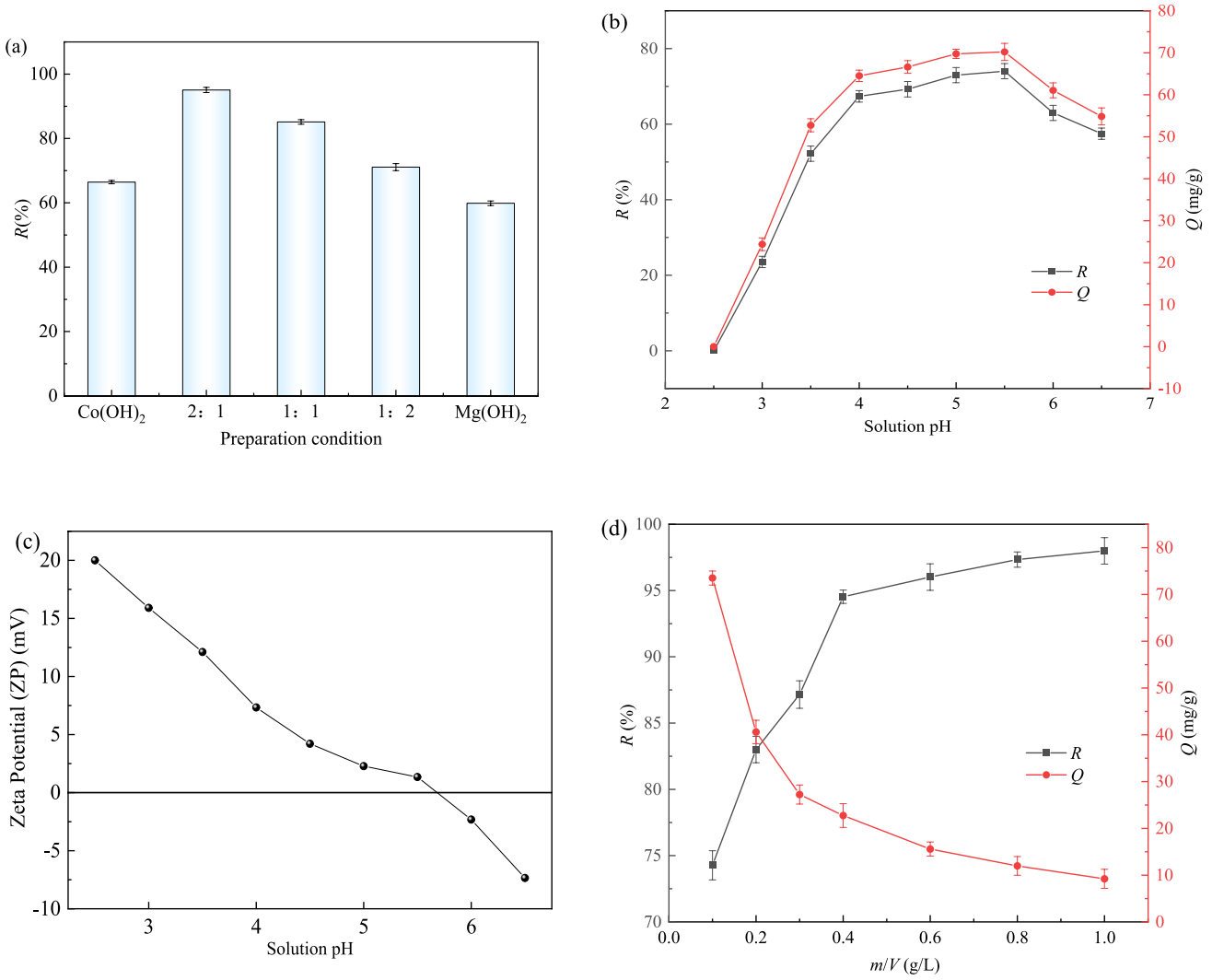

Fig. 4 (Color online) **a** Effect of the preparation conditions, **b** solution pH (*T*: 25 °C, *t:* 60 min, U(VI) concentration: 10 mg/L, dosage: 0.1 g/L), **c** Zeta potential characterization results, **d** Effect of dosage (*T*: 25 °C, *t:* 60 min, U(VI) concentration: 10 mg/L, solution pH: 5.5)

adsorption capacity were 94.59% and 23.23 mg/g, respectively. The removal rate increased slowly until the adsorbent dosage was 1 g/L, which corresponded to the highest removal rate; however, the adsorption capacity decreased to 9.62 mg/g. This may be because although more materials effectively increased the number of active sites, the number of unused active sites increased as well, resulting in a lowered unit adsorption capacity. Considering its cost-effectiveness, an adsorbent dosage of 0.4 g/L was optimal.

3.2.2 Effect of anions, cations and organic matter

Figure 5a and b shows the effects of the cations and anions on the removal efficiency of U(VI). Figure 5a shows that K^+ and Na^+ slightly affects the removal of U(VI), whereas Ca^{2+} significantly affects the removal efficiency. This may be attributed to the higher valence state and larger ion radius of Ca^{2+}, which result in strong competitive adsorption with U(VI) and ion exchange with the adsorbed U(VI) [46, 47], thereby affecting the removal efficiency.

As shown in Fig. 5b, the anions had a certain effect on the removal. CO_3^{2-} and SO_4^{2-} combine with UO_2^{2+} in solution to form $UO_2(CO_3)_2^{2-}$ and $UO_2(SO_4)_2^{2-}$ complexes, causing steric hindrance to uranium adsorption and resulting in a decrease in the removal rate [48, 49]. Combined with the zeta potential, the material surface exhibits a weak positive potential, while NO_3^- generates an electrostatic attraction with the material, undergoes coordination exchange, occupies the active sites on the material surface, and lowers the removal rate [50, 51].

Humic acid was chosen to study the effect of organic matter on U(VI) removal by the L-CMs. As shown in Fig. 5c, humic acid significantly affects the removal of U(VI) from aqueous solutions during the entire reaction

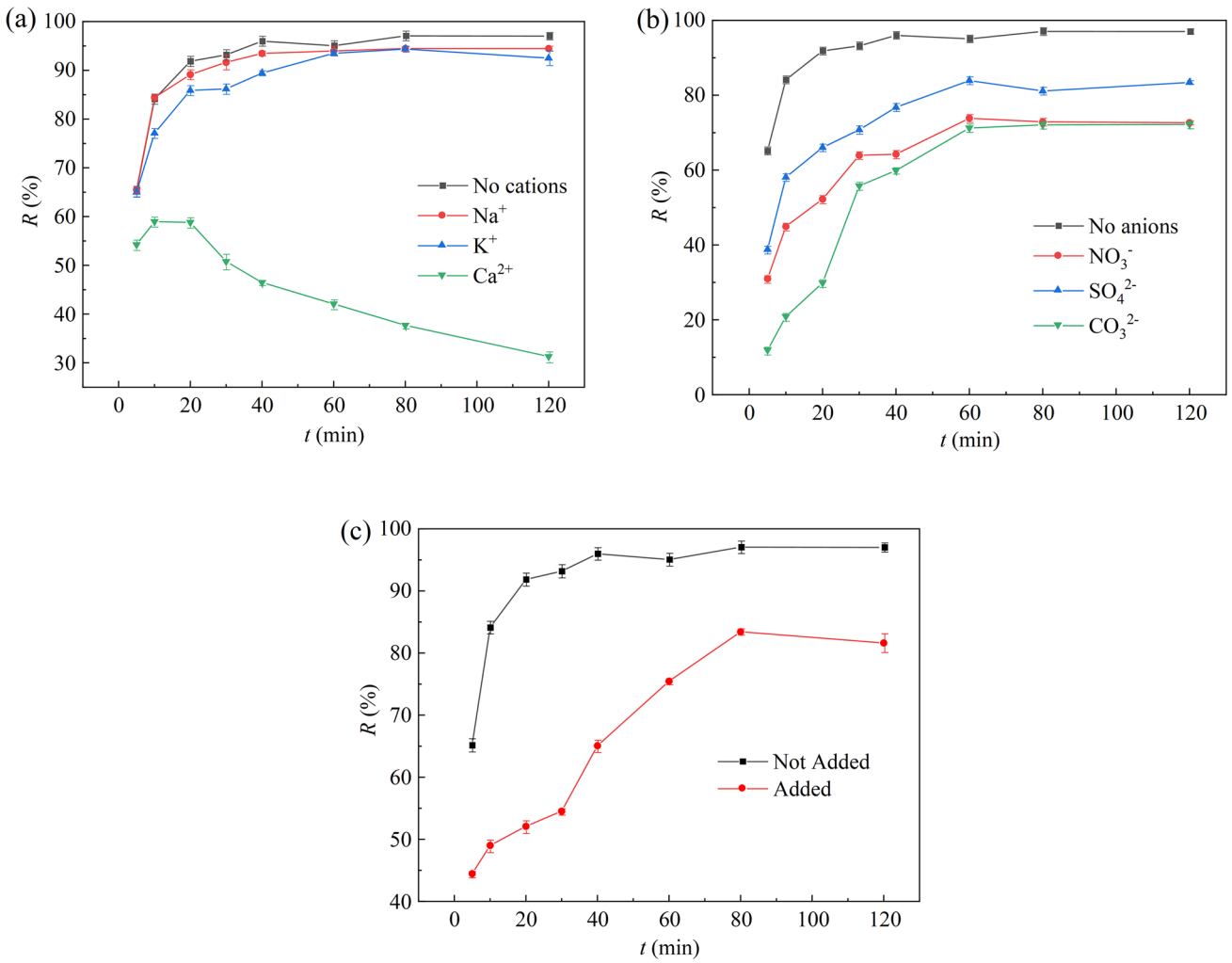

Fig. 5 (Color online) Effect of **a** cation, **b** anion, **c** humic acid (*t:* 60 min; U(VI) concentration: 10 mg/L, dosage: 0.4 g/L, *T:* 25 °C)

period. This may be attributed to the abundant carboxyl and hydroxyl functional groups in humic acid, which form complexes with the metal ions in the material to cover the surface of the active sites of the L-CMs and hinder the reaction [52].

3.3 Mechanism of U(VI) removal from solution by L-CMs

3.3.1 Adsorption kinetics

Kinetic adsorption studies provide important information regarding adsorption performance, rate of adsorption systems, and possible reaction mechanisms [53]. The effect of reaction times on adsorption is shown in Fig. 6a. The adsorption capacity is significantly affected by the reaction time. The adsorption capacity gradually increases with time; the adsorption trend is significant in the early stage and then slowly increased until equilibrium is attained. This is due to the higher U(VI) content in the solution in the early stage of the reaction, which facilitates the use of active sites on the surface of the material. The active sites on the surface of the L-CMs are then occupied, resulting in a slow increase in the removal rate until equilibrium. The pseudo-first-order, pseudo-second-order, and Elovich kinetic fitting analyses of the test results are presented in Fig. 6b and Table S1. According to the fitting results, the R^2 of the pseudo-second-order adsorption kinetic model is better than those of the remaining kinetic models. Thus, the adsorption of U(VI) by the L-CMs is consistent with pseudo-second-order kinetics, indicating that chemical adsorption occurs primarily.

3.3.2 Adsorption isotherm

The Langmuir, Freundlich, Temkin, and Redlich–Peterson (R–P) isothermal adsorption models were used to analyze

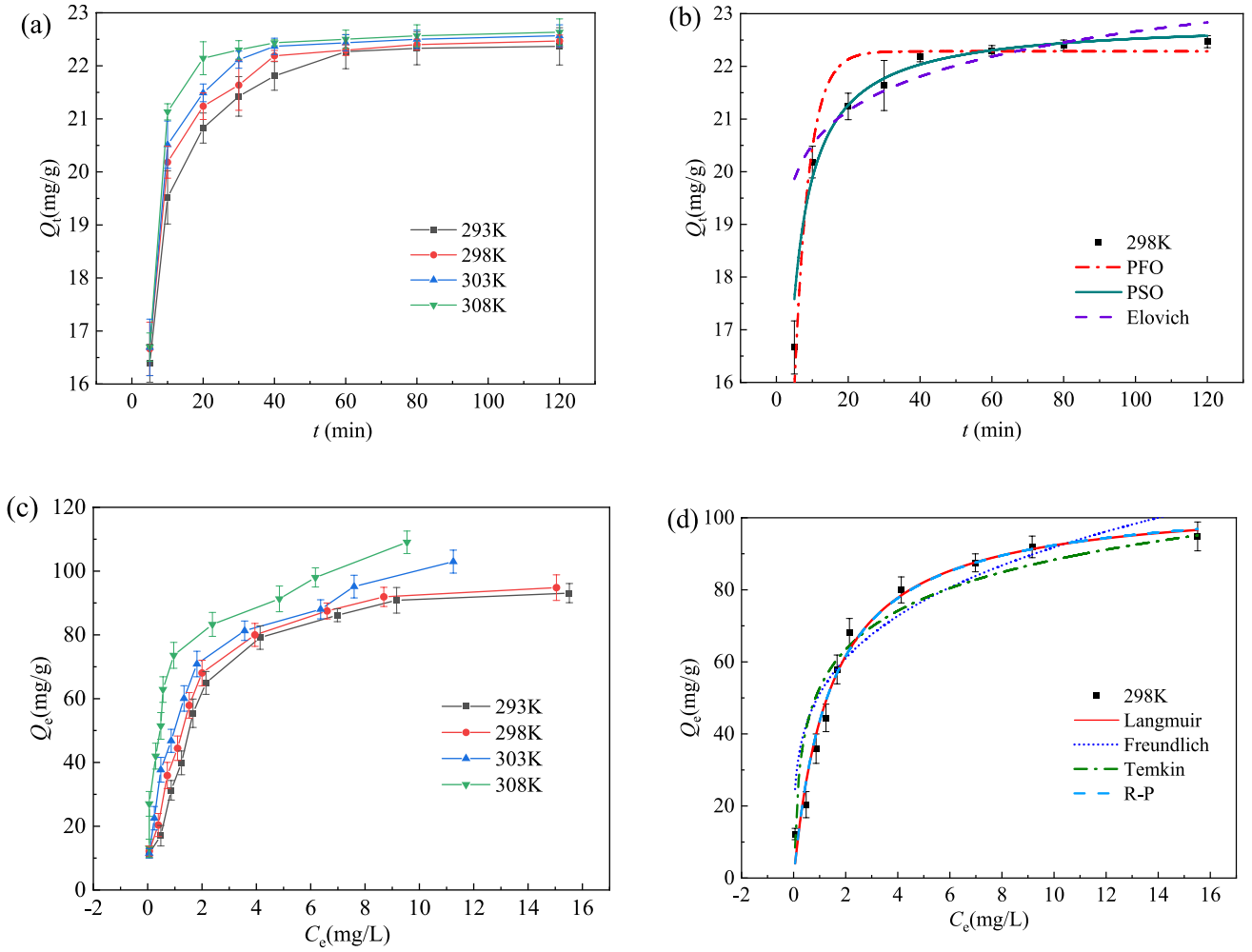

Fig. 6 (Color online) **a** Effect of contact time on the adsorption of U(VI) in solution, **b** adsorption kinetic models fitting, **c** adsorption isotherm, **d** adsorption isotherm models fitting

the adsorption of U(VI) by the L-CMs. Figure 6c shows the isothermal adsorption curves at different temperatures, while Fig. 6d shows the adsorption isotherm model fitting at room temperature (298 K). Figure 6d shows that the Langmuir model exhibits a high degree of fitting. The adsorption process conformed to the Langmuir adsorption isotherm model, that is, the monolayer adsorption occurred, and the maximum adsorption capacity was 105.49 mg/g at room temperature. Moreover, when $n = 1$, the R–P model was simplified to the Langmuir model [54]. Table S2 shows that $n = 0.99$, confirming that the process conformed to the Langmuir adsorption isotherm model. The Temkin isotherm provided well-fitted data, with an R^2 value of 0.938. In the Freundlich isotherm adsorption model, the $1/n$ value in Table S2 was less than 1, indicating that adsorption occurred easily.

3.3.3 Thermodynamic investigation

Based on the experimental data obtained at different temperatures and concentrations, a thermodynamic study of U(VI) adsorption by L-CMs was conducted, and the results are presented in Table S3. At different initial concentrations of U(VI), ΔH^0 was positive, indicating that the adsorption of U(VI) in solution by the L-CMs was an endothermic process. ΔS^0 was positive, indicating that the adsorption involved an irreversible reaction of disordered entropy increase, whereas ΔG^0 was negative, indicating that the adsorption process was spontaneous.

According to Table S4, at constant reaction temperatures, the value of E value gradually decreased with the increasing initial concentration of the solution within a certain concentration range. This is attributed to the fixed amount of the L-CMs added during the reaction, which fixed the number of active sites provided by the material. When the

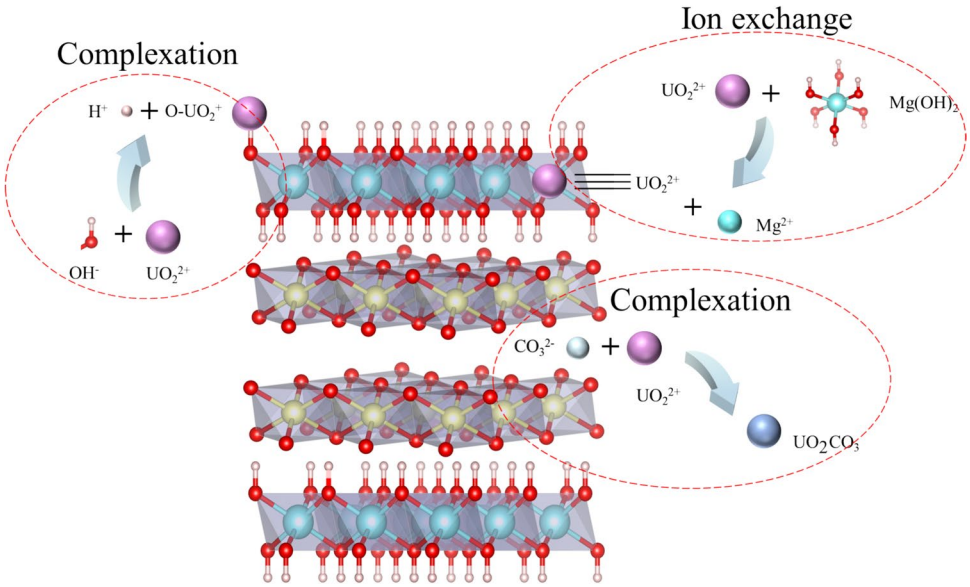

Fig. 7 (Color online) Mechanism model

Table 1 Comparison of the adsorption performance of the L-CMs with adsorbents in literatures

Adsorbent	Solution pH	Equilibrium time (min)	Q_{max}(mg/g)	References
Silane coupling agent modified bentonite (KH550-B)	5.0	50	20.24	[54]
Cetyl trimethyl ammonium bromide/Chitosan composited modified bentonite (CTAB/CTS-B)	7.0	120	20.84	[55]
Cetyl trimethyl ammonium bromide modified bentonite (CTAB-B)	6.9	355	27.25	[56]
Dodecyl trimethyl ammonium bromide modified bentonite (DTAB-B)	4.0	240	34.45	[58]
Ca-Al hydrotalcite (Ca-Al LDHs)	–	–	54.79	[59]
L-CMs	5.5	120	105.49	This work

concentration increased, U(VI) in the solution exceeded the number of available active sites, resulting in decreasing E values. When the initial concentration of U(VI) in the solution was constant, E gradually increased with temperature, further demonstrating that higher temperatures favored the removal of U(VI) by the L-CMs.

3.3.4 Mechanism model

The adsorption of U(VI) by the L-CMs was influenced by several factors, with chemical and physical adsorption playing primary and secondary roles, respectively. The adsorption mechanism is illustrated in Fig. 7, based on previously reported literature [55, 56] and the analysis presented in this paper.

XPS analysis showed that the peak position of elemental Co remained almost unchanged, whereas the peak area of Mg1s decreased and the peak position shifted, indicating an exchange between Mg^{2+} and UO_2^{2+}. This exchange is represented by Eq. (3). Furthermore, the results of the XPS and FTIR analyses demonstrated complexation between the -OH and CO_3^{2-} groups in the L-CMs material with UO_2^{2+}, as depicted in Eqs. (4) and (5).

$$\equiv Mg^{2+} + UO_2^{2+} \rightarrow \equiv UO_2^{2+} + Mg^{2+} \tag{3}$$

$$A{-}O{-}H + UO_2^{2+} \rightarrow A{-}O{-}UO_2^{+} + H^{+} \tag{4}$$

$$CO_3^{2-} + UO_2^{2+} \rightarrow UO_2CO_3 \tag{5}$$

3.4 Comparison of adsorption performance

Table 1 compares the adsorption capacity of the L-CMs for U(VI) with those of materials reported recently [20, 21, 57–59]. Considering the low solution pH of uranium-containing wastewater in practical engineering, the solution pH is an important factor that must be considered when evaluating the optimum adsorption capacity [8, 57]. Although the DTAB-B adsorbent achieved optimal removal performance at a solution pH of 4.0, it reached a maximum adsorption

capacity of only 34.45 mg/g after prolonged adsorption at room temperature. KH550-B achieved the optimal removal performance at a pH of 5.0, and the adsorption time was short; however, its maximum adsorption capacity was only 20.24 mg/g. The solution pH value for the best removal performance of the other adsorbents was close to neutral, which contradicted the actual application, and the maximum adsorption capacity was insignificant. Therefore, compared to other methods, the L-CMs exhibited a better removal performance.

4 Conclusion

In this study, a novel L-CMs was successfully prepared by introducing Co^{2+} between $Mg(OH)_2$ layers through a one-step co-precipitation method to remove U(VI) from radioactive wastewater. Characterizations of the structure and removal performance of the L-CMs demonstrated that the L-CMs possessed excellent U(VI) adsorption capacity. At room temperature and a solution pH of 5.5, the fitted maximum adsorption capacity was 105.49 mg/g. The U(VI) removal mechanism by the L-CMs may involve ion exchange between Mg^{2+} and UO_2^{2+}, and the complexation of -OH and CO_3^{2-} with UO_2^{2+} to remove U(VI) from aqueous solutions. Both the Co and Mg in this work were divalent; unlike traditional bimetallic hydroxides composed of divalent and trivalent metals, the L-CMs synthesized from divalent metals demonstrated superior U(VI) adsorption ability, which could broaden the future research scope of metal hydroxides. Moreover, the L-CMs exhibited excellent reusability, providing a new perspective for the effective removal of U(VI) from aqueous solutions.

Supplementary Information The online version contains supplementary material available at https://doi.org/10.1007/s41365-026-01886-6.

Author contributions All authors contributed to the study conception and design. Material preparation, data collection, and analysis were performed by Meng-Yue Ma, Yi-Shuo Zhang, Kun Li, Guan-Chao Li, Hao-Nan Li, Xiao-Liang Liu, Yan-Jun Du, Muhammad Saeed, Xiao-Yan Li, Yu-Hui Liu, and Yi-Bao Liu. The first draft of the manuscript was written by Meng-Yue Ma, and all authors commented on previous versions of the manuscript. All authors read and approved the final manuscript.

Data availability The data that support the findings of this study are openly available in Science Data Bank at https://cstr.cn/31253.11.sciencedb.j00186.00895 and https://doi.org/10.57760/sciencedb.j00186.00895.

Declarations

Conflict of interest The authors declare that they have no competing interests.

References

1. Y.F. Liu, S. Ni, W.J. Wang et al., Facile and scalable synthesis of functionalized hierarchical porous polymers for efficient uranium adsorption. Water Res. **257**, 121683 (2024). https://doi.org/10.1016/j.watres.2024.121683
2. Z. Dong, W.J. Yuan, C. Liu et al., Th(IV) and U(VI) removal by TODGA in ionic liquids: extraction behavior and mechanism, and radiation effect. Nucl. Sci. Tech. **28**, 62 (2017). https://doi.org/10.1007/s41365-017-0214-y
3. Q.H. Gao, J.T. Hu, R. Li et al., Radiation synthesis of a new amidoximated UHMWPE fibrous adsorbent with high adsorption selectivity for uranium over vanadium in simulated seawater. Radiat. Phys. Chem. **122**, 1–8 (2016). https://doi.org/10.1016/j.radphyschem.2015.12.023
4. X.L. Wei, H. Li, X. Zhang et al., Adsorption performance and mechanism of waste paper-derived phosphorus-rich carbon for separation of uranium from radioactive wastewater. J. Environ. Chem. Eng. **12**, 112486 (2024). https://doi.org/10.1007/s41365-017-0214-y
5. H. Zhang, Y.Y. Ao, Y. Wang et al., Effect of radiolysis of TODGA on the extraction of TODGA/n-dodecane toward Eu(III): an experimental and DFT study. Nucl. Sci. Tech. **34**, 48 (2023). https://doi.org/10.1007/s41365-023-01198-z
6. Y. Li, P. Ren, Y. Zhang et al., Synthesis of acrylonitrile composite material for the adsorption of uranium. J. East China U. Tech. **42**, 433–437 (2019). https://doi.org/10.3969/j.issn.1674-3504.2019.04.019
7. L. Ding, C.Y. Tao, S. Zhang et al., One-step synthesis of phosphorich, silica-enhanced chitosan aerogel for the efficient adsorption of uranium(VI). Int. J. Biol. Macromol. **259**, 129101 (2024). https://doi.org/10.1016/j.ijbiomac.2023.129101
8. M.Y. Ma, Y.S. Zhang, X.Y. Li, Removal of U(VI) from aqueous solution by Al^0/Ni^0 bimetallic material. Res. Chem. Intermed. **50**, 4485–4501 (2024). https://doi.org/10.1007/s11164-024-05356-9
9. S. Lin, Y.W. Fu, B. Na et al., Property and mechanism of in-situ mineralization of uranyl ions with calcium hydrogen phosphate. J. East China U. Tech. **45**, 275–281 (2022). https://doi.org/10.3969/j.issn.1674-3504.2022.03.009
10. Y.W. Fu, S.F. Zou, S. Zhang et al., Preparation of alginate fixed tannic acid biofilm membranes and its uranium adsorption behavior. J. East China U. Tech. **46**, 316–324 (2023). https://doi.org/10.3969/j.issn.1674-3504.2023.03.013
11. X. Xu, X.J. Ding, J.X. Ao et al., Preparation of amidoxime-based PE/PP fibers for extraction of uranium from aqueous solution. Nucl. Sci. Tech. **30**(2), 20 (2019). https://doi.org/10.1007/s41365-019-0543-0
12. Y.W. Cai, M. Fang, B.W. Hu et al., Efficient extraction of U(VI) ions from solutions. Nucl. Sci. Tech. **34**, 2 (2023). https://doi.org/10.1007/s41365-022-01154-3
13. W. He, Q.X. Xiao, Z.L.M. Qiu et al., Synergistic piezo-photocatalytic reduction of U(VI) by $Zn_{0.7}Cd_{0.3}S$ solid solution homojunction. Chem. Eng. J. **494**, 152947 (2024). https://doi.org/10.1016/j.cej.2024.152947
14. Z.H. Yang, J.X. Ma, F. Liu et al., Mechanistic insight into pH-dependent adsorption and coprecipitation of chelated heavy metals by in-situ formed iron (oxy)hydroxides. J. Colloid Interface Sci. **608**, 864–872 (2022). https://doi.org/10.1016/j.jcis.2021.10.039
15. Y.H. Liu, J.Y. Zhao, T. Bo et al., Enhanced uranium extraction via charge dynamics and interfacial polarization in MoS_2/GO heterojunction electrodes. Small **20**, 2401374 (2024). https://doi.org/10.1002/smll.202401374
16. W.N. Ren, X.X. Feng, Y.L. He et al., Branched fibrous amidoxime adsorbent with ultrafast adsorption rate and high amidoxime

utilization for uranium extraction from seawater. Nucl. Sci. Tech. **34**, 90 (2023). https://doi.org/10.1007/s41365-023-01237-9
17. J.J. Yang, J.N. Nie, L. Bian et al., Clay minerals/sodium alginate/polyethylene hydrogel adsorbents control the selective adsorption and reduction of uranium: experimental optimization and Monte Carlo simulation study. J. Hazard. Mater. **468**, 133725 (2024). https://doi.org/10.1016/j.jhazmat.2024.133725
18. W. Yin, M. Liu, Y.H. Wang et al., Fe_3O_4–$Mg(OH)_2$ nanocomposite as a scavenger for silver nanoparticles: rational design, facile synthesis, and enhanced performance. Environ. Res. **212**, 113292 (2022). https://doi.org/10.1016/j.envres.2022.113292
19. D.Z. Yuan, S.A. Zhang, L.L. Chen et al., Solvothermal synthesis of nanoporous polymer adsorbent bearing phosphine oxide for the removal of uranium strong acid media. J. East China U. Tech. **43**, 179–186 (2020). https://doi.org/10.3969/j.issn.1674-3504.2020.02.013
20. Y.S. Zhang, Z.K. Zhou, S.J. Yang et al., Adsorption performance of KH550 modified bentonite at low concentrations of U(VI). Nonferrous Met. Eng. **12**, 154–164 (2022). https://doi.org/10.3969/j.issn.2095-1744.2022.09.21
21. X. Fan, Removal and mechanism of uranium containing wastewater by cetyltrimethylammonium bromide/chitosan composite modified bentonite. China Nonferrous Metall. **52**, 126–137 (2023). https://doi.org/10.19612/j.cnki.cn11-5066/tf.2023.02.016
22. Z. Wang, J.F. Su, T.B. Zhao et al., Enhanced removal of fluoride from groundwater using biosynthetic hydroxyapatite modified by bimetallic (La–Fe or La–Al) hydroxides. J. Clean. Prod. **436**, 140649 (2024). https://doi.org/10.1016/j.jclepro.2024.140649
23. J. Yang, T.Y. Liang, B.Y. Panet, A spherical adsorbent produced from a bagasse biochar chitosan assembly for selective adsorption of platinum-group metals from wastewater. Int. J. Biol. Macromol. **266**, 131142 (2024). https://doi.org/10.1016/j.ijbiomac.2024.131142
24. F.R. Peligro, I. Pavlovic, R. Rojas et al., Removal of heavy metals from simulated wastewater by in situ formation of layered double hydroxides. Chem. Eng. J. **306**, 1035 (2016). https://doi.org/10.1016/j.cej.2016.08.054
25. Y. Wang, Y. Zhang, X.L. Liu et al., Construction of polydopamine-functionalized phosphate-intercalated Mg single bond Fe layered double hydroxide for efficient removal of U(VI). J. Water Process. Eng. **55**, 104074 (2023). https://doi.org/10.1016/j.jwpe.2023.104074
26. T. He, Q. Li, T. Lin et al., Recent progress on highly efficient removal of heavy metals by layered double hydroxides. Chem. Eng. J. **462**, 142041 (2023). https://doi.org/10.1016/j.cej.2023.142041
27. G.H. Li, M. Li, X. Zhang et al., Hydrothermal synthesis of zeolites-calcium silicate hydrate composite from coal fly ash with co-activation of $Ca(OH)_2$-NaOH for aqueous heavy metals removal. Int. J. Min. Sci. Technol. **32**, 563–573 (2022). https://doi.org/10.1016/j.ijmst.2022.03.001
28. C. Pan, Q. Xu, L.X. Zhou et al., Pseudocapacitive enhancement of brucite-like β-Co(OH)2 nanoflakes after the removal of intercalated water. J. Solid State Chem. **324**, 124110 (2023). https://doi.org/10.1016/j.jssc.2023.124110
29. Z. Wang, X. Liang, Z.R. Liu et al., Self-powered electrochemical water treatment system for pollutant degradation and bacterial inactivation based on high-efficient $Co(OH)_2$/Pt electrocatalyst. Nano Res. **16**, 2192–2198 (2023). https://doi.org/10.1007/s12274-022-4978-y
30. J.J. Qi, J.Z. Liu, F.B. Sun et al., High active amorphous $Co(OH)_2$ nanocages as peroxymonosulfate activator for boosting acetaminophen degradation and DFT calculation. Chin. Chem. Lett. **32**, 1814–1818 (2021). https://doi.org/10.1016/j.cclet.2020.11.026
31. N. Akram, J. Guo, W.L. Ma et al., Synergistic catalysis of $Co(OH)_2$/CuO for the degradation of organic pollutant under visible light irradiation. Sci. Rep. **10**, 1939 (2020). https://doi.org/10.1038/s41598-020-59053-9
32. Z.W. Gao, T. Zhang, M.N. Pervez et al., "Switch to love, switch to kill" - the interaction of Co-doped $La(OH)_3$ and peroxymonosulfate achieved highly efficient As(III) removal in water. Chem. Eng. J. **473**, 145410 (2023). https://doi.org/10.1016/j.cej.2023.145410
33. D.M. Jiang, Y.H. Yang, C.T. Huang et al., Removal of the heavy metal ion nickel (II) via an adsorption method using flower globular magnesium hydroxide. J. Hazard. Mater. **373**, 131–140 (2019). https://doi.org/10.1016/j.jhazmat.2019.01.096
34. B.W. Li, M.L. Tang, P. Wang et al., A new method of alkalinity remediation for Cd-contaminated groundwater by PAAS-modified $MgCO_3$/$Mg(OH)_2$ colloid. Chemosphere **359**, 142200 (2024). https://doi.org/10.1016/j.chemosphere.2024.142200
35. S.Y. Tian, Progress for treatment of wastewater containing heavy metals. J. Salt Lake Res. **20**, 67–72 (2012).
36. Y. Zhao, S. Ni, Y.Y. Liu et al., Structural and interfacial microenvironment modulation of two-dimensional layered niobium phosphate to enhance uranium adsorption. Desalination **583**, 117623 (2024). https://doi.org/10.1016/j.desal.2024.117623
37. Z.R. Hou, J. Yu, X.S. Zhou et al., Enhanced performance of hybrid supercapacitors by the synergistic effect of $Co(OH)_2$ nanosheets and NiMn layered hydroxides. J. Colloid Interface Sci. **646**, 753–762 (2023). https://doi.org/10.1016/j.jcis.2023.05.128
38. Y.J. Wang, J.J. Lin, Y.H. Wang et al., Highly efficient and selective removal of low-concentration antibiotics from aqueous solution by regenerable $Mg(OH)_2$. J. Environ. Sci. **87**, 228–237 (2020). https://doi.org/10.1016/j.jes.2019.06.017
39. H.N. Wang, L.M. Zhou, X.Q. Ao et al., Ion-imprinted macroporous polyethyleneimine incorporated chitosan/layered hydrotalcite foams for the selective biosorption of U(VI) ions. Int. J. Biol. Macromol. **266**, 131113 (2024). https://doi.org/10.1016/j.ijbiomac.2024.131113
40. P. Cheng, Z.Y. Wei, Y. Arbid et al., Insights into the performance and mechanism of Cr(VI) and U(VI) removal in water using innovative cross-linked chitosan adsorbent. J. Environ. Chem. Eng. **12**, 111731 (2024). https://doi.org/10.1016/j.jece.2023.111731
41. X.X. Feng, C. Li, X.Z. Mao et al., Efficient and selective removal of Pb(II) from landfill leachate using L-serine-modified polyethylene/polypropylene nonwoven fabric synthesized via radiation grafting technique. Nucl. Sci. Tech. **35**, 78 (2024). https://doi.org/10.1007/s41365-024-01440-2
42. J.Q. Li, J. Huang, Y. Chen et al., Adsorption of uranium by thiophene loaded nano zero-valent iron. J. East China U. Tech. **45**, 282–287 (2022). https://doi.org/10.3969/j.issn.1674-3504.2022.03.010
43. M.Z. Li, Y.S. Zhang, X.Y. Li, Performance and mechanism of uranium (VI) removal from aqueous solution by zero-valent nickel@hollow glass particles (ZVNi@HGP). Phys. Scr. **99**, 075961 (2024). https://doi.org/10.1088/1402-4896/ad5516
44. T. Xiong, Q.C. Li, J. Liao et al., Highly enhanced adsorption performance to uranium(VI) by facile synthesized hydroxyapatite aerogel. J. Hazard. Mater. **423**, 127184 (2022). https://doi.org/10.1016/j.jhazmat.2021.127184
45. Y.H. Liu, Y.N. Lu, S. Zhang et al., Amphiphilic ligand in situ assembly of uranyl active sites and selective interactions of molybdenum disulfide. J. Hazard. Mater. **442**, 130089 (2023). https://doi.org/10.1016/j.jhazmat.2022.130089
46. Z. Yishuo, Z. Zhongkui, Li. Longxiang, Study on adsorption effect and mechanism of uranium by hydroxyapatite modified bentonite. Acta Materiae Compositae Sinica **40**, 6740–6755 (2023). https://doi.org/10.13801/j.cnki.fhclxb.20230314.003

47. Y. Yin, G.Y. Xu, Y.X. Xu et al., Adsorption of inorganic and organic phosphorus onto polypyrrole modified red mud: evidence from batch and column experiments. Chemosphere **286**, 121862 (2022). https://doi.org/10.1016/j.chemosphere.2021.131862
48. T. Xiong, L.Y. Jia, Q.C. Li et al., Highly efficient adsorptive extraction of uranium from wastewater by novel kaolin aerogel. Sci. Total. Environ. **842**, 156916 (2022). https://doi.org/10.1016/j.scitotenv.2022.156916
49. J. Liao, L. Ding, Y. Zhang et al., Efficient removal of uranium from wastewater using pig manure biochar: understanding adsorption and binding mechanisms. J. Hazard. Mater. **423**, 127190 (2022). https://doi.org/10.1016/j.jhazmat.2021.127190
50. X.Q. Zheng, A.L. Wei, Y.X. Zhang et al., Characteristic of nitrate adsorption in aqueous solution by iron and manganese oxide / biochar composites. Environ. Sci. **39**, 1220–1232 (2018). https://doi.org/10.13227/j.hjkx.201704216
51. Y. Ge, Y. Wang, Y.Q. Chen et al., Electrically driven enhancement on selective adsorption of nitrate by microporous carbon from wastewater: synergism of functional groups and micropores. Chem. Eng. J. **495**, 153462 (2024). https://doi.org/10.1016/j.cej.2024.153462
52. Y.F. Liu, S. Li, W.J. Wang et al., Facile and scalable synthesis of functionalized hierarchical porous polymers for efficient uranium adsorption. Water Res. **257**, 121683 (2024). https://doi.org/10.1016/j.watres.2024.121683
53. S.C. Zhang, S.Y. Ning, J. Zhou et al., New insight into the adsorption of ruthenium, rhodium, and palladium from nitric acid solution by a silica-polymer adsorbent. Nucl. Sci. Tech. **31**, 34 (2020). https://doi.org/10.1007/s41365-020-0744-6
54. J.L. Wang, G. Xuan, Adsorption isotherm models: classification, physical meaning, application and solving method. Chemosphere **258**, 127279 (2020). https://doi.org/10.1016/j.chemosphere.2020.127279
55. Y.D. Guo, Z.H. Gong, C.X. Li et al., Efficient removal of uranium (VI) by 3D hierarchical Mg/Fe-LDH supported nanoscale hydroxyapatite: a synthetic experimental and mechanism studies. Chem. Eng. J. **392**, 123682 (2024). https://doi.org/10.1016/j.cej.2019.123682
56. M. Jafari, F. Ganjali, R. Eivazzadeh-Keihan et al., Recent advances in applications of graphene-layered double hydroxide nanocomposites in supercapacitors and batteries. FlatChem. **45**, 100658 (2024). https://doi.org/10.1016/j.flatc.2024.100658
57. P. Das, A. Debnath, Fabrication of $MgFe_2O_4$/polyaniline nanocomposite for amputation of methyl red dye from water: isotherm modeling, kinetic and cost analysis. J. Disper. Sci. Technol. **44**, 14 (2022). https://doi.org/10.1080/01932691.2022.2110110
58. Y.S. Zhang, Z.K. Zhou, S.J. Yang et al., Adsorption of low conteration U(VI) in wasterwater with CTAB modified bentonite. Hydrometallurgy of China **41**, 145 (2022). https://doi.org/10.13355/j.cnki.sfyj.2022.02.011
59. L.Y. Li, J. Wang, Z.S. Li et al., Ultrasound assisted synthesis of Ca–Al hydrotalcite for U(VI) and Cr(VI) adsorption. Chem. Eng. J. **218**, 295–302 (2013). https://doi.org/10.1016/j.cej.2012.12.051